

Multistage Phase Decomposition Behavior and Kinetics for $Zr_{65}Ni_{30}Pd_5$ Ternary Amorphous Alloy

E. Shalaan^{a,*}, A. Inoue^{a,b,c}, F. Al-Marzouki^a, S. Al-Heniti^a, A. Y. Obaid^d, S. Al-Hashmi^a

^aDepartment of Physics, King Abdulaziz University, Jeddah, Saudi Arabia

^bInstitute of Massive Amorphous Metal Science, China University of Mining Technology, Xuzhou, China

^cInternational Institute of Green Materials, Josai International University, Togane, Japan

^dDepartment of Chemistry, King Abdulaziz University, Jeddah, Saudi Arabia

Received: October 23, 2019; Revised: November 03, 2019; Accepted: November 11, 2019.

We have examined heating-induced phase decomposition and its kinetics for $Zr_{65}Ni_{30}Pd_5$ amorphous alloy in an argon atmosphere. The amorphous phase decomposes through three stages in the order of amorphous \rightarrow icosahedral quasicrystal (I-Q) + amorphous \rightarrow approximant cubic $Zr_2(Ni,Pd) \rightarrow$ tetragonal Zr_2Ni + tetragonal Zr_2Pd phases. The approximant crystalline (APC) $Zr_2(Ni,Pd)$ phase includes icosahedral-like local atomic arrangements and the structural similarity between the I-Q and APC phases seems to enable the multistage phase decomposition through the precipitation of the APC phase. The primary precipitation of the I-Q phase from the amorphous phase occurs through nucleation and growth mechanisms through two-dimensional (2D) growth mode at lower heating rate and 3D growth mode at a high heating rate.

Keywords: *Metallic glass, Approximant crystals, Amorphous Alloy, Quasicrystalline.*

1. Introduction

The three transition metals Zr, Ni and Pd have high negative heats of mixing with hydrogen and hence the ternary Zr-Ni-Pd amorphous alloys are expected to exhibit a high hydrogen absorption ability.¹⁻⁹ On the other hand, the reactivity with oxygen for the ternary alloys is much larger for Zr, while that for Pd is negligible. Thus, the ternary amorphous alloys have attracted an increasing interest as unique materials in the reactivity with gas elements as well as in the dealloying to fabricate a nanoporous Pd(Ni) structure.

Although there are some papers on the oxidation-induced crystallization behavior for the Zr-Ni-Pd ternary amorphous alloys,¹⁻⁴ little is known about the crystallization behavior of the ternary amorphous alloys in an inert gas atmosphere. This situation is significantly different from the academic background that there are a number of papers on the crystallization behavior of Zr-Pd binary,¹⁰⁻¹⁷ and Zr-Ni-Pd ternary amorphous alloys.¹⁸⁻²⁴ The difference is presumably because an icosahedral quasicrystalline (I-Q) phase is formed as a primary precipitation phase in the crystallization process for $Zr_{65-70}Pd_{25-30}$ binary and $Zr_{70}Ni_{10}Pd_{20}$ ternary amorphous alloys.¹⁰⁻²⁴ The crystallization of the binary amorphous alloys occurs through two stages in the process of amorphous \rightarrow I-Q + residual amorphous \rightarrow equilibrium tetragonal Zr_2Pd phase. The addition of late transition metals (LTM) such as Fe, Co, Ni and Cu to Zr-Pd binary alloys is expected to enhance the amorphous forming ability through the multicomponent effect leading to the atomic size mismatches of $Zr > Pd > LTM$. Furthermore, the significant atomic size mismatches are thought to be effective for the increase in the thermal stability of metastable phases of amorphous and I-Q phases.

The increase in the stability through the sluggish decomposition reaction of their metastable phases may enable the appearance of the approximant crystalline (APC) phase which lies in an intermediate stage in the aspects of atomic configuration and internal energy between I-Q and equilibrium crystalline phases. The searching for a new amorphous alloy composition where the three metastable phases of amorphous, I-Q and APC phases appear in a simple ternary alloy is very meaning for basic science and engineering aspects to develop useful metastable materials. There have been no data on any binary and ternary amorphous alloys with the crystallization process where the three metastable phases appear. The finding is expected to deep the interpretation on the role of the atomic size mismatch effect in the formation tendency of their three metastable phases, though the satisfaction of only the atomic size factor cannot enhance the thermal stability of supercooled liquid which enables the formation of bulk metallic glasses.

The precipitation of I-Q phase from glassy phase has been reported in a number of alloy systems such as Zr-Cu,^{19,23} Zr-M (M=Pd or Pt),¹⁰⁻¹⁷ Zr-Ni-M (M=Pd, Au or Pt),¹⁸⁻²⁴ Zr-Al-Ni-Cu^{20,22} and Zr-Cu-Ni-Pd²¹ glassy alloys, while the transition from I-Q phase to APC phase remains unknown even for their typical I-Q formation glassy alloys where the three component rule for stabilization of supercooled liquid as well as the formation of bulk metallic glasses is satisfied. Very recently, we have noticed that the sequent transition of the three metastable phases, namely, amorphous \rightarrow I-Q \rightarrow APC \rightarrow equilibrium crystalline phases occurs in a very simple $Zr_{65}Ni_{30}Pd_5$ ternary amorphous alloy.

*e-mail: eshalaan@yahoo.com

In addition, the multicomponent Zr-Ni-Pd alloy gives a unique opportunity to investigate the possibility of synthesizing a glass-type alloy with glass transition and supercooled liquid region. This is because the alloy component deviates slightly from the three component rule for stabilization of supercooled liquid and bulk glass formation.^{20,21}, i.e., the satisfaction of significant atomic size mismatches of $Zr > Pd > Ni$, while the deviation of the bonding state resulting from the coexistence of the nearly zero heat of mixing for Ni-Pd atomic pair and the negative heats of mixing for Zr-Ni and Zr-Pd pairs. This paper aims to examine the thermal stability, phase decomposition behavior and kinetics of a $Zr_{65}Ni_{30}Pd_5$ amorphous alloy and to investigate the feature of the phase decomposition for the ternary amorphous alloy in comparison with the I-Q precipitation behavior for $Zr_{70}Pd_{30}$ and $Zr_{65}Pd_{35}$ binary amorphous alloys,¹⁸⁻²² as well as for Zr-Ni-Pd ternary amorphous alloys.¹⁸⁻²⁴

2. Experimental Details

An alloy ingot with the nominal atomic composition of $Zr_{65}Ni_{30}Pd_5$ was chosen because the ternary alloy is expected to increase the thermal stability of metastable phases through the atomic size mismatch effect as compared with binary Zr-Ni and Zr-Pd alloys. The ingot was prepared by arc melting the mixture of pure Zr, Ni and Pd metals with purity above 99.9 mass% in an argon atmosphere.

Alloy ribbon with a cross section of about $0.02 \times 1.2 \text{ mm}^2$ was prepared by the single roller melt spinning method with a high-frequency induction furnace in an argon environment. The diameter of the copper wheel was 200 mm and the wheel rotation speed was 3000 rpm.

Amorphicity and annealed structures were identified and examined by X-ray diffraction (XRD) using Rigaku SmartLab X-ray diffractometer with $CuK\alpha$ radiation. Thermal stability, crystallization behavior and kinetics were examined by differential scanning calorimetry (DSC) (Perkin Elmer DSC 8500) at heating rates of 0.083 – 1.33 K/s. Annealing treatment was made for 2 hrs at 423-523 K in an argon atmosphere using one zone programmable furnace from MTI Corporation, model OTF1200X.

3. Results

Figure 1 shows DSC curves of the $Zr_{65}Ni_{30}Pd_5$ amorphous alloy in the as-spun state and the pre-heated states at 423 K, 473 K and 523 K with a scanning rate of 0.333 K/s. No appreciable glass transition is observed in the temperature range just below the onset temperature of crystallization, indicating the formation of an amorphous type phase. The as-spun and pre-annealed samples exhibit three exothermic peaks, indicating that the amorphous phase completes its crystallization through three stages.

The three-stage exothermic behavior remains unchanged even after the pre-annealing for 2 hrs at the temperatures below 523 K. The three-stage exothermic peak behavior is different from the two-stage exothermic behavior for $Zr_{70}Ni_{30}$, $Zr_{70}Pd_{30}$ and $Zr_{70}Ni_{10}Pd_{20}$ amorphous alloy ribbons.¹⁸⁻²⁴ The two-stage crystallization for these amorphous alloys can be interpreted to originate from the decrease of thermal stability through easy atomic diffusivity and atomic rearrangements for the alloys without the multicomponent effect such as atomic size mismatch.

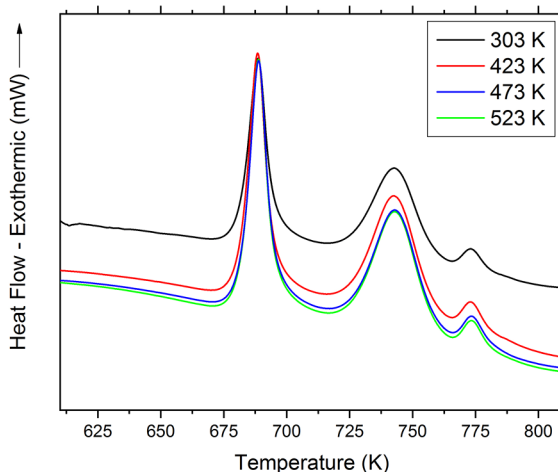


Figure 1. DSC curves for $Zr_{65}Ni_{30}Pd_5$ amorphous alloy in as-spun (303 K) and pre-annealed (423, 473 and 523 K) states.

With the aim of clarifying the precipitation phases corresponding to each exothermic peak, Fig. 2 shows the XRD patterns of the as-spun and the annealed samples heated at 0.333 K/s to 700 K (just above the first exothermic peak), 763 K (above the second peak) and 785 K (above the third peak). These XRD patterns can be recognized as an amorphous phase in the as-spun state, I-Q and residual amorphous phases at 700 K, approximant cubic Zr_2Ni phase with a lattice parameter of 1.12 nm at 763 K, and two mixed compounds of tetragonal Zr_2Ni with $a=0.654 \text{ nm}$ and $c=0.534 \text{ nm}$ and tetragonal Zr_2Pd with $a=0.3299 \text{ nm}$ and $c=1.088 \text{ nm}$. Based on the DSC and XRD data, it is concluded that the crystallization of the $Zr_{65}Ni_{30}Pd_5$ amorphous alloy occurs through the multistage process of amorphous \rightarrow I-Q + amorphous \rightarrow APC $Zr_2Ni(Pd) \rightarrow Zr_2Ni + Zr_2Pd$. It is noticed that the metastable I-Q and APC cubic $Zr_2(Ni,Pd)$ phases precipitate only for the ternary amorphous alloy and this three-stage phase decomposition process is significantly different from the two-stage crystallization mode for binary Zr-Ni and Zr-Pd or even for the ternary $Zr_{70}Ni_{10}Pd_{20}$ amorphous alloys. The Ni-Pd atomic pair has a nearly zero heat of mixing and the Ni-Pd equilibrium phase diagram is a typical solid soluble type.¹⁰⁻²⁴ The homogeneously mixed state is presumed to be the origin of the suppression of the directly separated precipitation mode to Zr_2Ni and Zr_2Pd phases.

The approximant crystalline (APC) $Zr_2(Ni,Pd)$ phase has a complex cubic structure with a lattice parameter of 1.12 nm including an icosahedral-like local atomic configuration. The similarity of the local atomic configuration in the I-Q and APC structures seems to cause the preferential precipitation of metastable APC $Zr_2(Ni,Pd)$ phase from the I-Q phase.

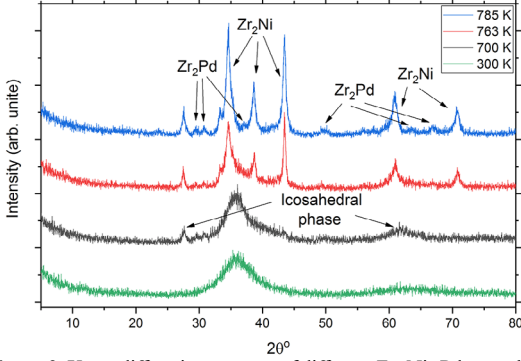


Figure 2. X-ray diffraction patterns of different $Zr_{65}Ni_{30}Pd_5$ samples; (a) as-spun and annealed for 900 s at (b) 700 K (c) 763 K and (d) 785 K. The identified phases are also presented.

It was thus shown that the addition of Ni causes a significant influence of crystallization mode in comparison with the $Zr_{65-70}Pd_{30-35}$ binary amorphous alloys. Here, we further examined the kinetic behavior of the I-Q precipitation from the ternary Zr-Ni-Pd amorphous phase, in comparison with the previous data on the Zr-Pd amorphous alloy.¹⁰⁻¹⁸ To gain some information about the conversion kinetics from the amorphous phase to I-Q phase, the quasicrystallized-volume fraction, α , should be determined. Here the Johnson–Mehl–Avrami model can be used to express, $\alpha(T)$ as follows:²⁵⁻²⁹

$$\alpha(T) = 1 - \exp[-(k(T)t)^n] \quad (1)$$

where t is the time, n is the kinetic exponent or Avrami exponent. The importance of n is because the mechanism and dimensionality of the quasicrystallization can be deduced from the value of n . $k(T)$ is constant (reaction rate) and can be described by the Arrhenius temperature dependence:

$$k(T) = k_0 \exp\left[-\frac{E_A}{RT}\right] \quad (2)$$

where k_0 is called as the frequency factor, E_A is the activation energy throughout the crystallization development, R is the ideal gas constant.

The reaction rate constant can be linked with the phase transformation rate $d\alpha/dt$ through the following relation:³⁰

$$\frac{d\alpha}{dt} = k(T)\zeta(\alpha) \quad (3)$$

where $\zeta(\alpha)$ is conversion function of the quasicrystallized volume fraction α . The function $\zeta(\alpha)$ can be described as follows:^{29,30}

$$\zeta(\alpha) = (1 - \alpha)[- \ln(1 - \alpha)]^{-\frac{1}{n}} \quad (4)$$

The above equation is derived without taking into account the isothermal limitation, and hence it should be used also to describe non-isothermal quasicrystallization kinetics.

Figure 3 shows DSC curves of $Zr_{65}Ni_{30}Pd_5$ amorphous alloy measured at different heating rates (non-isothermal). It is clear that the position of each peak is shifted toward upper temperatures, as the heating rate is increased. In the non-isothermal process, the quasicrystallized volume fraction, α , is deduced from the thermal analysis curves as a function of the measured temperature. The volume fraction quasicrystallized, α , at a given temperature T is calculated by:³¹

$$\alpha(T) = \frac{A_T}{A} \quad (5)$$

where A is the total area under the exothermic peak between the temperatures T_0 and T_∞ that correspond to the beginning and end of crystallization development, respectively. A_T is the partial area under the exothermic peak from T_0 up to the temperature T . For simplicity, only the first exothermic peak due to the formation of I-Q phase is considered. The calculated quasicrystallization volume fractions are shown in Fig. 4. All the curves exhibit a sigmoidal reliance with temperature which is normal for all amorphous materials during the non-isothermal crystallization process.

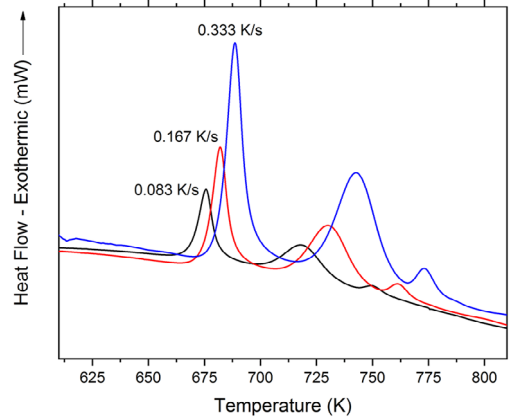


Figure 3. Non-isothermal DSC curves obtained at different heating rates.

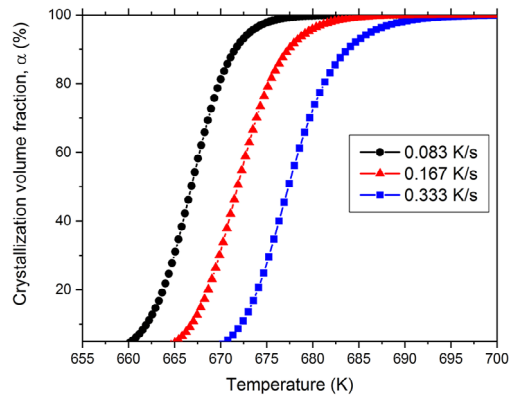


Figure 4. Non-isothermal crystallization volume fraction, α as a function of temperature.

The values of kinetic parameter n and the rate constants $k(T)$ are deduced from nonlinear fits of the recorded data, using Eqs. 1 and 2. As summarized in Table 1, the average values of n are 1.93 at the heating rate of 0.083 K/s, 2.25 at 0.167 K/s and 2.63 at 0.333 K/s, respectively. Since n acquires only integer values from 1 to 4, here n values at 0.083 K/s and 0.167 K/s are close to 2 corresponding to 2-dimensional growth of quasicrystals, while the n value at 0.333 K/s becomes close to 3, implying nearly three-dimensional quasicrystallization growth.

With the aim of evaluating the activation energy for the precipitation of I-Q phase, plots of $\ln k(T)$ against $1/T$ are shown in Fig. 5. Good linear relations are recognized at 0.083, 0.167 and 0.333 K/s and the activation energies evaluated from the linear slope are about 1.65, 1.70 and 1.78 kJ/mol, respectively, as shown in Table 1.

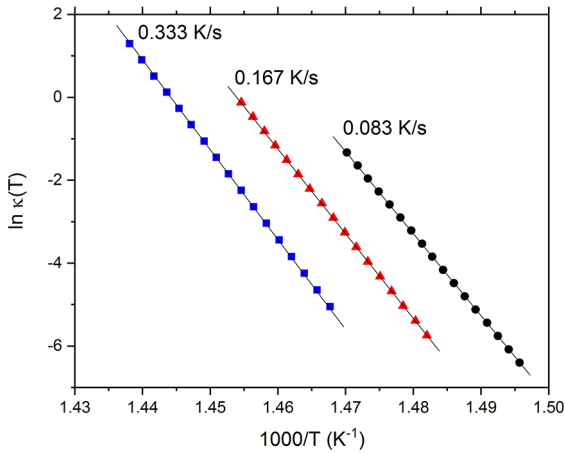


Figure 5. Plots of $\ln k(T)$ versus $1/T$ (under non-isothermal process).

Figure 6 shows DSC curves of the $Zr_{65}Ni_{30}Pd_5$ amorphous alloy under an isothermal crystallization condition obtained at various annealing temperatures. It can be easily observed that the exothermic peak-time decreases with increasing annealing temperature. This is due to the fact that the atoms have larger mobility at superior annealing temperature that guides to easy formation flux for mass quasicrystallization.³² These results agree well with the previous reports for Pd-, Zr- and Cu-based bulk glassy alloys.³³⁻³⁶

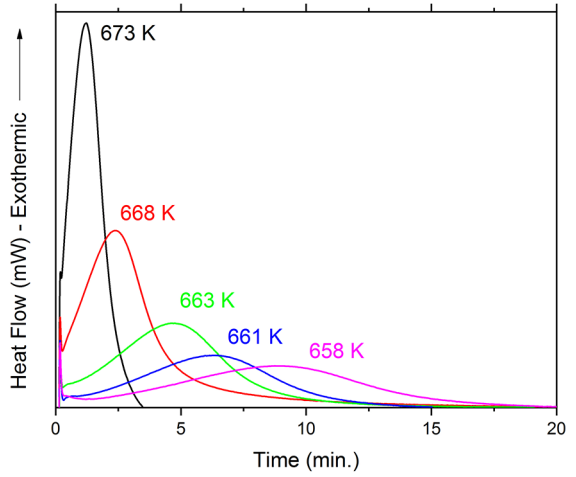


Figure 6. Isothermal DSC curves obtained at different annealing temperatures.

The correspondence involving the crystallization volume fraction and annealing time through isothermal development is revealed in Fig. 7. It is clearly shown that all the curves display a characteristic s-shaped type at all annealing temperatures and that with increasing annealing temperature the phase transformation process goes more rapidly. It is observed that the amorphous phase transfers into two kinds of metastable phases of I-Q and approximant cubic $Zr_2(Ni,Pd)$ before stable tetragonal Zr_2Ni and Zr_2Pd phases.

By combining Eqs. 3 and 4, and taking the logarithm of the resulting equation, the following equation is obtained:

$$\ln\left(\frac{d\alpha}{dt}\right) - \ln(1 - \alpha) = \ln(k(T)) + \left(\left(1 - \frac{1}{n}\right)\ln(-\ln(1 - \alpha))\right) \quad (6)$$

Scheming of $\ln\left(\frac{d\alpha}{dt}\right) - \ln(1 - \alpha)$ versus $\ln(-\ln(1 - \alpha))$ at different annealing temperatures is displayed in Fig. 8. The kinetic parameter n and the reaction rate $K(T)$ can be estimated from the fitted curves. The obtained values of n are given in Table 2.

Table 1. Non-isothermal kinetic parameters for $Zr_{65}Ni_{30}Pd_5$ at different heating rates.

	0.083 K/s	0.167 K/s	0.333 K/s
n	1.93 ± 0.086	2.25 ± 0.118	2.63 ± 0.177
E_A (kJ/mol)	1652.5 ± 65.387	1704.1 ± 85.846	1784.2 ± 94.88
ΔH (J/g)	-44.95	-55.50	-63.37

Table 2. Isothermal kinetic parameters for $Zr_{65}Ni_{30}Pd_5$ at different temperatures.

	673 K	668 K	661 K	658 K
n	2.43 ± 0.01	2.13 ± 0.02	2.78 ± 0.08	2.79 ± 0.07
E_A (kJ/mol)	1191.2 ± 69.36	1135.2 ± 70.16	1058.2 ± 86.08	1017.8 ± 92.34
ΔH (J/g)	-30.06	-22.42	-19.25	-18.50

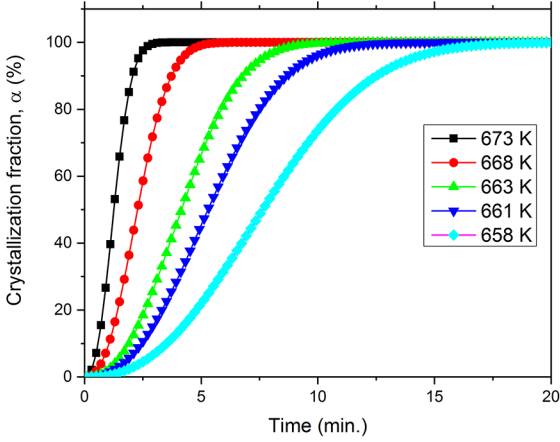


Figure 7. Crystallization volume fraction α as a function of annealing time at different annealing temperatures.

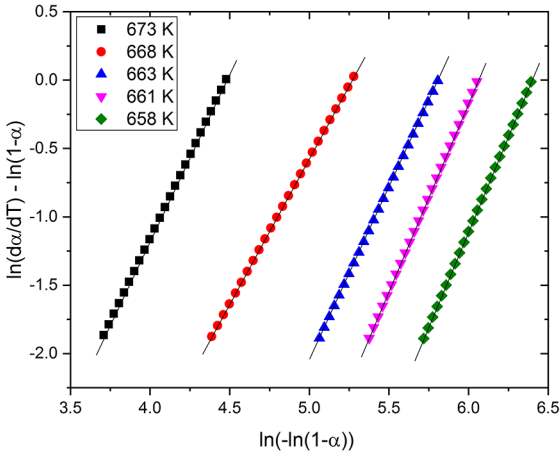


Figure 8. Plots of $\ln\left(\frac{d\alpha}{dT}\right) - \ln(1-\alpha)$ versus $\ln(-\ln(1-\alpha))$ at different annealing temperatures.

As summarized in Table 2, n diverges from 2.1 to 2.8 with increasing annealing temperature. Similar disparity has been observed in other bulk glassy alloys.³⁷⁻⁴¹ This disparity is somewhat narrow. According to the theory of diffusion controlled growth,³⁷ n may take the following values: $n=1.5$, $1.5 < n < 2.5$, $n=2.5$ and $n > 2.5$ which correspond to the following cases: i- the growth of particles occurs with a nucleation rate close to zero, ii- decreasing nucleation rate, iii- constant nucleation rate, and iv- increasing nucleation rate, respectively.³⁹ Here the average kinetic exponent n is 2.53 which means that the growth of I-Q particles in the $Zr_{65}Ni_{30}Pd_5$ amorphous alloy happens with a constant nucleation rate. The similar value of n has also been reported for $Zr_{55.9}Cu_{18.6}Ta_{8.7}Al_{7.5}Ni_{10}$.⁴⁰

Using the Arrhenius equation (2), the activation energy for the quasicrystallization development in an isothermal process can be obtained. Plots of $\ln k(T)$ versus $1/T$ are displayed in Fig. 9. All fitted curves are straight lines and coincide. The calculated activation energies are summarized in Table 2.

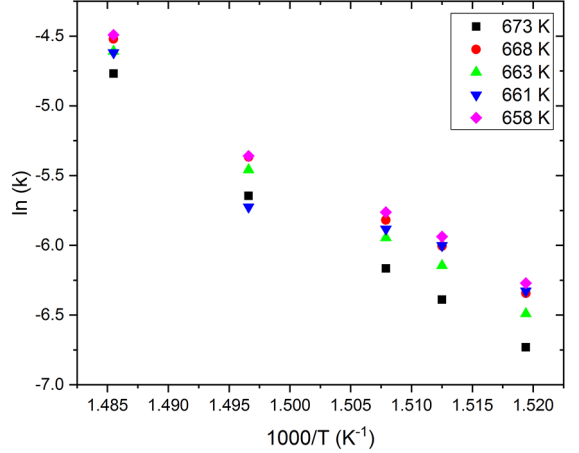


Figure 9. Plots of $\ln k(T)$ versus $1/T$ (under isothermal process).

Here, the calculated activation energies under isothermal conditions are smaller than the values calculated under non-isothermal conditions (during a continuous heating). This occurrence is in contrary to other results observed in different bulk glassy alloys.⁴¹⁻⁴³ Nucleation and growth are two phenomena which take place in the crystallization process. In the non-isothermal condition nucleation is predominant, since crystallization initiates at low temperatures. While in the isothermal condition, equally nucleation and growth are dominant with the same attribution during crystallization. Thus, in the $Zr_{65}Ni_{30}Pd_5$ amorphous alloy, the energy barrier in non-isothermal annealing condition is higher than that of isothermal conditions.

4. Discussion

It was shown in the present study that the decomposition of $Zr_{65}Ni_{30}Pd_5$ amorphous phase upon continuous heating or isothermal annealing occurs in the order of amorphous, I-Q, cubic $Zr_2Ni(Pd)$ and then $Zr_2Ni + Zr_2Pd$ phases, instead of the two-stage process of amorphous, I-Q and then tetragonal Zr_2Ni or Z_2Pd without APC cubic $Zr_2(Ni,Pd)$ phase. Considering that the Zr-Ni and Zr-Pd amorphous alloys crystallize through two stages,¹³⁻¹⁷ the appearance of the three metastable amorphous, I-Q and APC phases is presumed to reflect the increase in the thermal stability of each metastable phase which is due to the sluggish phase decomposition reaction resulting from the difficulty of atomic rearrangements caused by the multicomponent effect leading to the distinct atomic size mismatches. Figure 10 shows a schematic illustration of continuous heating decomposition behavior of the $Zr_{65}Ni_{30}Pd_5$ amorphous phase. It is noticed that the I-Q phase does not decompose directly to stable crystalline mixed phases. The formation of the metastable APC cubic $Zr_2Ni(Pd)$ phase seems to reflect the ease of the phase transition of I-Q phase resulting from the structural similarity in local atomic configurations between the I-Q and the $Zr_2(Pd,Ni)$ phases and the APC cubic phase has a close relation with I-Q phase.

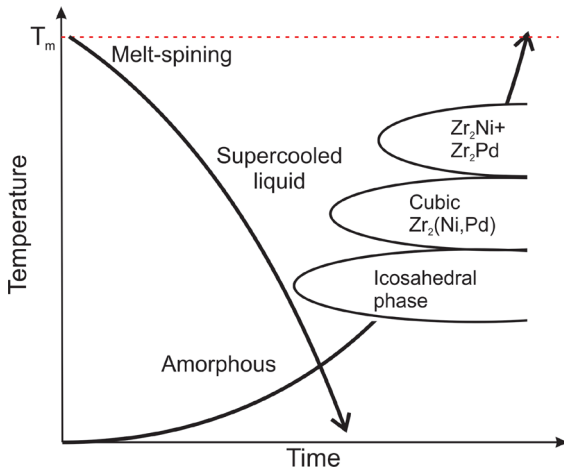


Figure 10. Schematic illustration of continuous-cooling-transformation (CCT) and continuous-heating-transformation (CHT) curves of $Zr_{65}Ni_{30}Pd_5$ amorphous alloy.

The internal energy of these metastable phases lowers in the order of amorphous > I-Q > cubic $Zr_2Ni(Pd)$ > tetragonal Zr_2Ni + tetragonal Zr_2Pd . The formation of the mostly single APC cubic $Zr_2Ni(Pd,Ni)$ phase from the I-Q phase is believed to be the first evidence in the decomposition behavior of the I-Q phase. It is interesting to point out that this alloy gives a unique opportunity to clarify the transformation behavior from I-Q to APC cubic $Zr_2Ni(Pd)$ phase in the absence of any other phase state as well as the coexistent and interface structures between I-Q and APC $Zr_2Ni(Pd)$ phases. The clarification is expected to shed on the light to the mutual phase relationships among amorphous, I-Q and APC $Zr_2Ni(Pd)$, which remain still unknown, and is under investigation.

5. Conclusions

The heating-induced decomposition behavior and its kinetics of $Zr_{65}Ni_{30}Pd_5$ amorphous alloy, which is attractive as a hydrogen absorption material, were examined in comparison with $Zr_{65-70}Pd_{30-35}$ binary amorphous alloys as well as $Zr_{70}Ni_{10}Pd_{20}$ ternary amorphous alloy. The amorphous phase decomposes through three stages of amorphous, I-Q + amorphous, APC cubic $Zr_2Ni(Pd)$ and then tetragonal Zr_2Ni + tetragonal Zr_2Pd , being different from the two-stage decomposition of amorphous, I-Q + amorphous and then tetragonal Zr_2Pd for $Zr_{65-70}Pd_{30-35}$ binary amorphous alloys. The formations of I-Q and APC cubic $Zr_2Ni(Pd)$ are presumably due to the development of icosahedral-like local atomic configurations in Zr-Ni-Pd amorphous alloy. The formation kinetics of the I-Q phase from the amorphous phase was also examined in continuous heating and isothermal annealing. The Avrami exponent n value increases from 1.93 at 0.083 K/s to 2.63 at 0.333 K/s in the continuous heating mode and is nearly constant in the isothermal annealing mode.

Based on these data, the decomposition from the amorphous to I-Q phase occurs through two-dimensional growth mode with a constant nucleation mechanism at lower heating rate and three-dimensional growth mode at a higher heating rate.

6. Acknowledgments

This project was funded by the National Plan for Science, Technology and Innovation (MAARIFAH) – King Abdulaziz City for Science and Technology - the Kingdom of Saudi Arabia – award number (12-NAN3196-03). The authors also, acknowledge with thanks Science and Technology Unit, King Abdulaziz University for technical support.

7. References

1. Yamaura S, Kimura H, Inoue A. Hydrogen absorption of oxide composite materials prepared from melt-spun Zr-Pd-Ni Alloys. *Materials Transactions*. 2003;44(4):696-699.
2. Arachi Y, Emura S, Omura A, Nunogaki M, Asai T, Yamaura S, et al. Structural analysis of nano-sized-Pd/ZrO₂ composite after H(D) absorption. *Solid State Ionics*. 2006;177(19-25):1861-1864.
3. Yamaura S, Sasamori K, Kimura H, Inoue A, Zhang YC, Arata Y. Hydrogen absorption of nanoscale Pd particles embedded in ZrO₂ matrix prepared from Zr-Pd amorphous alloys. *Materials Research*. 2002;17(6):1329-1334.
4. Inoue A, Wang Z, Louzguine-Luzgin DV, Han Y, Kong FL, Shalaan E, et al. Effect of high-order multicomponent on formation and properties of Zr-based bulk glassy alloys. *Journal of Alloys and Compounds*. 2015;638:197-203.
5. Caron A, Zhang QS, Minkow A, Zadorozhny VA, Fukuhara M, Fecht HJ, et al. Mesostructural effects on the mechanical properties of Zr-based bulk metallic glasses. *Materials Science and Engineering: A*. 2012;555:57-62.
6. Ketov SV, Shi X, Xie G, Kumashiro R, Churyumov AY, Bazlov AI, et al. Nanostructured Zr-Pd metallic glass thin film for biochemical applications. *Scientific Reports*. 2015;5:7799.
7. Köster U, Jastrow L, Zander D. Oxidation of Zr-TM metallic glasses. *Journal of Metastable and Nanocrystalline Materials*. 2003;15-16:49-60.
8. Caron A, Kawashima A, Fecht HJ, Louzguine-Luzgin DV, Inoue A. On the anelasticity and strain induced structural changes in a Zr-based bulk metallic glass. *Applied Physics Letters*. 2011;99(17):171907.
9. Qiang JB, Zhang W, Xie GQ, Inoue A. Unusual room temperature ductility of a Zr-based bulk metallic glass containing nanoparticles. *Applied Physics Letters*. 2007;90(23):231907.
10. Saida J, Matsushita M, Inoue A. Direct observation of icosahedral cluster in $Zr_{70}Pd_{30}$ binary glassy alloy. *Applied Physics Letters*. 2001;79(3):412.
11. Saida J, Matsushita M, Inoue A. Nanoscale icosahedral quasicrystalline phase formation in a rapidly solidified $Zr_{80}Pt_{20}$ binary alloy. *Applied Physics Letters*. 2000;77(1):73-75.

12. El-Eskandarany MS, Saida J, Inoue A. Amorphization and crystallization behaviors of glassy Zr₇₀Pd₃₀ alloys prepared by different techniques. *Acta Materialia*. 2002;50(10):2725-2736.
13. Saida J, Matsushita M, Li C, Inoue A. Formation of the icosahedral quasicrystalline phase in Zr₇₀Pd₃₀ binary glassy alloy. *Philosophical Magazine Letters*. 2001;81(1):39-44.
14. Saida J, Matsushita M, Inoue A. Nanoicosahedral quasicrystalline phase in Zr–Pd and Zr–Pt binary alloys. *Journal of Applied Physics*. 2001;90(9):4717-4724.
15. Imafuku M, Saida J, Inoue A. Change in local atomic structure during formation of the icosahedral quasicrystalline phase in Zr₇₀Pd₃₀ glassy alloy. *Materials Research*. 2001;16(1):3046-3049.
16. Saida J, Matsushita M, Inoue A. Nano icosahedral phase in Zr–Pd and Zr–Pt binary alloys. *Journal of Alloys and Compounds*. 2002;342(1):18-23.
17. Kitada M, Imafuku M, Saida J, Inoue A. Structural study of quasicrystallization in Zr–M (M=Pd or Pt) metallic glasses. *Journal of Non-Crystalline Solids*. 2002;312-314:594-598.
18. Saida J, Matsushita M, Li C, Inoue A. Formation of icosahedral quasicrystalline phase in Zr₇₀Ni₁₀M₂₀ (M=Pd, Au, Pt) ternary metallic glasses. *Applied Physics Letters*. 2000;76(24):3558-3560.
19. Saida J, Kasai M, Matsubara E, Inoue A. Stability of glassy state in Zr-based glassy alloys correlated with nano icosahedral phase formation. *Annales de Chimie Science des Matériaux*. 2002;27(5):77-89.
20. Saida J, Matsushita M, Inoue A. Nano icosahedral quasicrystals in Zr-based glassy alloys. *Intermetallics*. 2002;10(11-12):1089-1098.
21. Saida J, Yamada R, Kozikowski P, Imafuku M, Sato S, Ohnuma M. Characterization of nano-quasicrystal-formation in correlation to the local structure in Zr-based metallic glasses containing Pd. *Journal of Alloys and Compounds*. 2017;707:46-50.
22. Saida J, Kato H, Setyawan AD, Yoshimi K, Inoue A. Nanostructure controlling in Zr-based metallic glasses using icosahedral local structure. *Journal of Alloys and Compounds*. 2009;483(1-2):231-234.
23. Saida J, Imafuku M, Sato S, Matsubara E, Inoue A. Local structure in quasicrystal-forming Zr-based metallic glasses correlated with a stability of the supercooled liquid state. *Journal of Non-Crystalline Solids*. 2007;353(32-40):3704-3708.
24. Saida J, Itoh K, Sanada T, Sato S, Imafuku M, Ohnuma M, et al. Atomic structure of nanoscale quasicrystal-forming Zr–noble metal binary metallic glasses. *Journal of Alloys and Compounds*. 2011;509(Suppl 1):S27-S33.
25. Liu CT, Chisholm MF, Miller MK. Oxygen impurity and microalloying effect in a Zr-based bulk metallic glass alloy. *Intermetallics*. 2002;10(11-12):1105-1112.
26. Inoue A. Stabilization of metallic supercooled liquid and bulk amorphous alloys. *Acta Materialia*. 2000;48(1):279-306.
27. Avrami M. Kinetics of Phase Change. II Transformation-Time Relations for Random Distribution of Nuclei. *The Journal of Chemical Physics*. 1940;8(2):212-224.
28. Avrami M. Granulation, Phase Change, and Microstructure Kinetics of Phase Change. III. *The Journal of Chemical Physics*. 1941;9(2):177-184.
29. Bruijn TJW, Jong WA, Van Den Berg PJ. Kinetic parameters in Avrami–Erofeev type reactions from isothermal and non-isothermal experiments. *Thermochemica Acta*. 1981;45(3):315-325.
30. Khawam A, Flanagan DR. Solid-state kinetic models: basics and mathematical fundamentals. *The Journal of Physical Chemistry B*. 2006;110(35):17315-17328.
31. Murty BS, Ping DH, Hono K, Inoue A. Icosahedral phase formation by the primary crystallization of a Zr–Cu–Pd metallic glass. *Scripta Materialia*. 2000;43(2):103-107.
32. Ray CS, Huang W, Day DE. Crystallization kinetics of a lithia–silica glass: effect of sample characteristics and thermal analysis measurement techniques. *Journal of American Ceramic Society*. 1991;74(1):60-66.
33. Qiao JC, Pelletier JM. Crystallization kinetics in Cu₄₆Zr₄₅Al₇Y₂ bulk metallic glass by differential scanning calorimetry (DSC). *Journal of Non-Crystalline Solids*. 2011;357(14):2590-2594.
34. Liu L, Zhao XJ, Ma CL, Zhang T. Kinetics of crystallization process for Pd-based bulk metallic glasses. *Intermetallics*. 2009;17(4):241-245.
35. Jang JSC, Chang LJ, Chen GL, Huang JC. Crystallization behavior of the Zr₆₃Al_{7.5}Cu_{17.5}Ni₁₀B₂ amorphous alloy during isothermal annealing. *Intermetallics*. 2005;13(8):907-911.
36. Prashanth KG, Scudino S, Surreddi KB, Sakaliyska M, Murty BS, Eckert J. Crystallization kinetics of Zr₆₅Ag₅Cu_{12.5}Ni₁₀Al_{7.5} glassy powders produced by ball milling of pre-alloyed ingots. *Materials Science and Engineering: A*. 2009;513-514:279-285.
37. Yang YJ, Xing DW, Shen J, Sun JF, Wei SD, He HJ, et al. Crystallization kinetics of a bulk amorphous Cu–Ti–Zr–Ni alloy investigated by differential scanning calorimetry. *Journal of Alloys and Compounds*. 2006;415(1-2):106-110.
38. Wang J, Kou HC, Li JS, Gu XF, Zhong H, Chang H, et al. An integral fitting method for analyzing the isochronal transformation kinetics: Application to the crystallization of a Ti-based amorphous alloy. *Journal of Physics and Chemistry of Solids*. 2009;70(11):1448-1453.
39. Scudino S, Venkatarama S, Eckert J. Thermal stability, microstructure and crystallization kinetics of melt-spun Zr–Ti–Cu–Ni metallic glass. *Journal of Alloys and Compounds*. 2008;460(1-2):263-267.
40. Chen Q, Liu L, Chan KC. Crystallization kinetics of the Zr_{55.9}Cu_{18.6}Ta₈Al_{7.5}Ni₁₀ bulk metallic glass matrix composite under isothermal conditions. *Journal of Alloys and Compounds*. 2006;419(1-2):71-75.
41. Okai D, Shimizu Y, Hirano N, Fukami T, Yamasaki T, Inoue A. Isothermal crystallization in supercooled liquid state for Ca₃₀Mg_{22.5}Cu_{27.5} metallic glass. *Journal of Alloys and Compounds*. 2010;504(Suppl 1):S247-S250.
42. Yang YJ, Xing DW, Shen J, Sun JF, Wei SD, He HJ, et al. Crystallization kinetics of a bulk amorphous Cu–Ti–Zr–Ni alloy investigated by differential scanning calorimetry. *Journal of Alloys and Compounds*. 2006;415(1-2):106-110.
43. Wei S, Ding B, Lei T, Hu Z. Crystallization of amorphous Zr₆₅Cu₂₇Al₈ alloy with wide supercooled liquid region. *Materials Letters*. 1998;37(4-5):263-267.